Mineralogical Magazine, June 2016, Vol. 80(4), pp. 547–565

On the compositional variability of dalyite, $K_2ZrSi_6O_{15}$: a new occurrence from Terceira, Azores

A. J. Jeffery[1,*], R. Gertisser[1], R. A. Jackson[1], B. O'Driscoll[1,2] and A. Kronz[3]

[1] School of Physical and Geographical Sciences, Keele University, Keele, Staffordshire ST5 5BG, UK
[2] School of Earth, Atmospheric and Environmental Sciences, The University of Manchester, Oxford Road, Manchester M13 9PL, UK
[3] Geowissenschaftliches Zentrum Göttingen, Goldschmidtstrasse 3, D-37077 Göttingen, Germany

[*Received 15 September 2014; Accepted 29 June 2015; Associate Editor: G. Diego Gatta*]

ABSTRACT

The rare potassium zirconium silicate dalyite has been identified for the first time on Terceira, Azores, within syenitic ejecta of the Caldeira-Castelinho Ignimbrite Formation. New quantitative analyses of this dalyite were combined with the small number of published analyses from various locations worldwide to evaluate the mineral's compositional variability. Additionally, solid-state modelling has been applied to assess the site allocations of substituting elements. The new analyses yield the average formula $(K_{1.84}Na_{0.15})_{\sum=1.99}(Zr_{0.94}Ti_{0.012}Hf_{0.011}Fe_{0.004})_{\sum=0.967}Si_{6.03}O_{15}$. Model results predict the placement of substituting Hf and Ti in the octahedral site, and highlight the overall complexity in the incorporation of Fe, Mg and Ba. The combined dataset reveals that dalyite found within peralkaline granites and syenites is generally defined by higher Na↔K substitution and lower Ti↔Zr substitution relative to dalyite from highly potassic rocks. The Terceira dalyite exhibits a bimodal variation in the degree of Na↔K substitution which is attributed to a K-enrichment trend induced by late-stage pore wall crystallization and albitization, coupled with the control of pore size upon the degree of supersaturation required to initiate nucleation of dalyite in pores of varying size.

Keywords: dalyite, peralkaline, syenite, oceanic island magmatism, Terceira, Azores.

Introduction

Dalyite is a rare potassium zirconium silicate, with the empirical formula $K_2ZrSi_6O_{15}$. It was first identified in peralkaline granitic ejecta found within the pyroclastic sequences of Green Mountain and Middleton Peak, Ascension Island (Van Tassel, 1952). Since its discovery, it has been identified as an accessory phase in a variety of rocks, including peralkaline granites and syenites, late-stage pegmatites, charoitites, lamproites, lamprophyres, fenites and carbonatites (e.g. Furnes *et al.*, 1982; Robins *et al.*, 1983; Harris and Rickard, 1987; Linthout *et al.*, 1988; Konev *et al.*, 1996). Having been established as a general indicator of peralkaline conditions, silica-oversaturation and high chemical potential of K_2O (μK_2O) (e.g. Marks *et al.*, 2011), the presence and composition of dalyite provides important insights into the evolution of these magmatic systems.

Here, we report the first known occurrence of dalyite from the mildly peralkaline rocks of Terceira, Azores. We apply solid-state modelling to investigate various proposed substituting elements, and complement the existing global database with new high-quality quantitative chemical analyses of dalyite from Terceira. Using these analyses, alongside whole-rock major-element analyses of the host syenites, we discuss the geochemical variability of dalyite, based on previously published compositions from both similar and contrasting rock types.

Background

Dalyite occurrences

Following the initial discovery of dalyite (Van Tassel, 1952), it was next identified in peralkaline syenitic

*E-mail: a.j.jeffery@keele.ac.uk
DOI: 10.1180/minmag.2016.080.018

ejecta from Agua de Pau volcano, São Miguel, Azores (Cann, 1967; Widom *et al.*, 1993), where it was observed as an entirely intercumulus phase and therefore inferred by Ridolfi *et al.* (2003) to be the last mineral to crystallize (alongside quartz). Lazebnik and Makhotko (1982) identified dalyite in the Murun Complex, Siberia, Russia, also providing additional quantitative analyses. Furnes *et al.* (1982) and Robins *et al.* (1983) noted the presence of dalyite within a highly potassic lamprophyric dyke in Sunnfjord, Norway. Raade and Mladeck (1983) reported dalyite within a peralkaline granite pluton at Gjerdingen, Norway, where it was found typically in close contact with janhaugite $Na_3Mn_3Ti_2Si_4O_{15}(OH,F,O)_3$. Harris and Rickard (1987) recorded the occurrence of dalyite, alongside eudialyte, in a peralkaline granitic dyke that cross-cuts the nepheline syenites of the Straumsvola Complex, Antarctica. In 1988, an enstatite-sanidine-phlogopite lamproite in south-eastern Spain was reported to contain the mineral's first known occurrence in an extrusive rock (Venturelli *et al.*, 1984; Linthout *et al.*, 1988). Soon afterwards, dalyite was observed within fenites from the Salitre–Serra Negra carbonatite-alkaline igneous complex, Brazil (Mariano and Francis, 1989; Mariano and Marchetto, 1991; Brod, 1999). Dalyite was later identified in the Strange Lake peralkaline granite complex, Canada, and noted to have nucleated heterogeneously onto older zircon crystals (Birkett *et al.*, 1992; Salvi and Williams-Jones, 1995). Subsequent reported occurrences include the Amis peralkaline granite intrusion of the Brandberg Complex, Namibia (Schmitt *et al.*, 2000), the various lithologies of the Murun Complex, Siberia, Russia (e.g. Dolivo-Dobrovol'skiy and Yevdokimov, 1991; Konev *et al.*, 1996; Reguir, 2001), the Gordon Butte pegmatites, Montana, USA (Chakhmouradian and Mitchell, 2002), peralkaline granite dykes to the north of the Zargat Na'am ring complex, Egypt (Saleh, 2006), more unusually, a nepheline-bearing pegmatite, Langesundfjord, Norway (Andersen *et al.*, 2010), and the alkali syenites and metasomatites of the Shibanovsky Massif, Russia (Stepnova *et al.*, 2013) (Fig. 1).

The occurrence documented here is within quartz syenite ejecta sampled from the Caldeira-Castelinho Ignimbrite Formation (CCI) on Terceira Island, Azores (Gertisser *et al.*, 2010). The nine Azorean islands straddle the Mid-Atlantic Ridge in the central North Atlantic Ocean and mark a triple junction between the North American, Eurasian and Nubian plates (e.g. Krause and Watkins, 1970). All nine islands are volcanic in origin and represent the subaerial manifestation of a large submarine plateau, itself interpreted to have originated from the interaction of a mantle plume with the Mid-Atlantic Ridge (e.g. Gente *et al.*, 2003). The CCI is one of at least seven ignimbrite formations found within the stratigraphy of Terceira (Self, 1974, 1976; Gertisser *et al.*, 2010) and can be readily distinguished from its counterparts by its relative abundance of quartz syenite ejecta (Gertisser *et al.*, 2010). The discovery of dalyite within these ejecta marks the mineral's second known occurrence within the Azores archipelago.

Mineral properties

Van Tassel (1952) provided the first description of the physical properties, chemical composition, unit-cell and powder x-ray diffraction data of dalyite. It is a triclinic, colourless mineral of moderate positive relief, exhibiting up to second order interference colours at 30 μm thickness. The unit cell was defined as $K_2ZrSi_6O_{15}$, though the potential substitutions of Na for K, and Hf for Zr, were suggested. The chemical similarity between dalyite and wadeite ($K_2ZrSi_3O_9$) was also noted. The original quantitative chemical analysis of dalyite is reported in Table 1 (analysis 1).

The crystal structure of dalyite was determined by Fleet (1965), who defined it as a phyllosilicate comprising four-, six- and eight-membered rings of SiO_4 tetrahedra. These sheets are linked by regular ZrO_6 octahedra and irregular $(K,Na)O_8$ polyhedra. Robins *et al.* (1983) provided ten quantitative chemical analyses of dalyite from Sunnfjord, Norway and presented evidence for the substitution of Zr with Ti, and K with Fe, suggesting the more accurate empirical formula $(K,Na,Fe)_2(Zr,Ti)Si_6O_{15}$. They also highlighted the compositional similarity between dalyite and darapiosite, $KNa_2LiMnZnZrSi_{12}O_{30}$, sogdianite, $(K,Na)_2Li_2(Li,Fe,Al,Ti)_2Zr_2(Si_2O_5)_6$ and zektzerite, $LiNaZrSi_6O_{15}$. Further chemical analyses of dalyite were reported by Harris *et al.* (1982), Lazebnik and Makhotko (1982), Harris and Rickard (1987), Linthout *et al.* (1988), Birkett *et al.* (1992), Konev *et al.* (1996), Reguir (2001), Chakhmouradian and Mitchell (2002) and Ridolfi *et al.* (2003) (Table 1).

Methods

Analytical procedure

Whole-rock major-element analyses of the syenite ejecta were undertaken at Acme Analytical

https://doi.org/10.1180/minmag.2016.080.018 Published online by Cambridge University Press

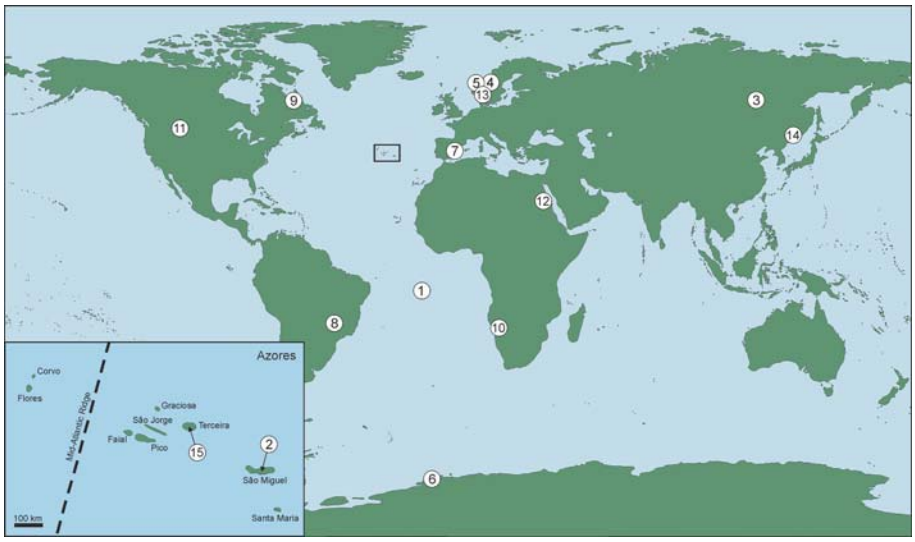

FIG. 1. Reported occurrences of dalyite worldwide. (1) Ascension Island, South Atlantic Ocean (Van Tassel, 1952); (2) Agua de Pau (or Fogo) volcano, São Miguel, Azores (Cann, 1967); (3) the Murun Complex, Siberia, Russia (Lazebnik and Makhotko, 1982; Dolivo-Dobrovol'skiy and Yevdokimov, 1991; Konev *et al.*, 1996; Reguir, 2001); (4) Gjerdingen, Norway (Raade and Mladeck, 1983); (5) Sunnfjord, Norway (Furnes *et al.*, 1982; Robins *et al.*, 1983); (6) the Straumsvola Complex, Dronning Maud Land, Antarctica (Harris and Rickard, 1987); (7) Cancarix, South Eastern Spain (Venturelli *et al.*, 1984; Linthout *et al.*, 1988); (8) the Serra Negra and Salitre Complex, Brazil (Mariano and Francis, 1989; Mariano and Marchetto, 1991); (9) the Strange Lake Complex, Canada (Birkett *et al.*, 1992; Salvi and Williams-Jones, 1995); (10) the Brandberg Complex, Namibia (Schmitt *et al.*, 2000); (11) Gordon Butte, Montana, USA (Chakhmouradian and Mitchell, 2002); (12) the Zargat Na'am ring complex, Egypt (Saleh, 2006); (13) Langesundfjord, Norway (Andersen, *et al.*, 2010); (14) the Shibanovsky Massif, Russia (Stepnova *et al.*, 2013); (15) Terceira Island, Azores (this study).

Laboratories Ltd, Canada, using x-ray fluorescence spectrometry (samples TER 30-1, TER 30-6, TER 35-1), and inductively coupled plasma – atomic emission spectroscopy (TER 30-7). Weathered surfaces were removed and samples were crushed in an agate mill, prior to drying for 2 h at 110°C and a $LiBO_2$ fusion. Loss-on-ignition (LOI) was reported as the weight difference after ignition for 2 h at 1000°C.

Semi-quantitative analyses and element maps were produced using a Hitachi TM-3000 scanning electron microscope equipped with a Bruker Quantax 70 energy-dispersive system at Keele University, UK. Quantitative major-element analyses of dalyite were achieved for samples TER 30-1 and TER 30-7 using a JEOL JXA 8900 RL electron microprobe at the Georg-August Universität Göttingen, Germany. Peak counting times were 15 s for Si, Ti, Al, Fe, Mg, Ca, Na and K, and 30 s for Cr, Zr, Hf, Mn and Ba, using an acceleration voltage of 15 kV, a beam current of 15 nA and a 20 μm defocused beam. The following natural silicate minerals and synthetic materials (denoted as formulae) were used as primary standards: olivine (Si, Mg), albite (Na), sanidine (K), TiO_2 (Ti), hematite (Fe), anorthite (Al), wollastonite (Ca), Cr_2O_3 (Cr), rhodonite (Mn), celsian (Ba), $ZrSiO_4$ (Zr) and $HfSiO_4$ (Hf). Detection limits and errors (Table 2) were calculated at a two-sigma confidence level from the raw background noise and the signal/background counting, respectively, following the Gaussian law of error propagation. Matrix corrections were applied by using the phi-rho-z algorithm of the *CITZAF* program of Armstrong (1995).

Solid-state modelling

Solid-state modelling calculations were carried out to investigate the substitution of a number of potential substituting cations (Ti, Hf, Fe, Ba and

https://doi.org/10.1180/minmag.2016.080.018 Published online by Cambridge University Press

TABLE 1. Electron-microprobe analyses of dalyite from the literature. Oxide values reported as wt.%, structural formulas calculated on the basis of 15 oxygens.

Location	Ascension	Ascension	Straumsvola	Strange Lake	Gordon Butte	Agua de Pau	Agua de Pau	Agua de Pau	Agua de Pau	Murun
Group	1	1	1	1	1	1	1	1	1	2
Host rock	Granite ejecta	Granite ejecta	Granite dyke	Granite	Alkaline pegmatite	Syenitic ejecta	Syenitic ejecta	Syenitic ejecta	Syenitic ejecta	
Suggested origin	Magmatic	Magmatic	Magmatic	Magmatic	Magmatic	Magmatic	Magmatic	Magmatic	Magmatic	Magmatic or Metasomatic
No.	1†	2*	3	4	5	6	7	8	9	10
SiO_2	61.85	63.25	62.07	62.55	60.35	62.23	61.35	61.35	61.36	63.62
TiO_2	-	0.12	0.13	0.08	1.78	0.08	0.11	0.14	0.15	1.87
Al_2O_3	-	-	-	bdl	bdl	-	-	-	-	0.03
FeO	0.33	0.03	bdl	0.06	0.18	-	-	-	-	bdl
MnO	-	bdl	bdl	-	bdl	-	-	-	-	-
MgO	-	-	-	-	bdl	-	-	-	-	-
CaO	-	bdl	bdl	bdl	bdl	-	-	-	-	0.02
Na_2O	1.75	0.79	bdl	bdl	0.02	0.69	0.37	0.44	0.49	0.11
K_2O	14.6	14.63	15.71	15.08	15.34	13.8	14.56	14.6	14.72	14.99
ZrO_2	21.7	20.43	20.63	20.38	18.21	23.72	23.57	23.27	23.49	21.5
HfO_2	-	-	-	0.81	-	-	-	-	-	-
BaO	-	-	-	-	bdl	-	-	-	-	bdl
P_2O_5	-	-	-	-	-	-	-	-	-	-
La_2O_3	-	bdl	bdl	0.04	-	-	-	-	-	-
Ce_2O_3	-	bdl	bdl	0.06	bdl	-	-	-	-	-
Nb_2O_5	-	bdl	bdl	-	1.65	-	-	-	-	-
Total	100.23	99.25	98.54	98.96	97.53	100.52	99.96	99.8	100.21	102.14
Si	5.94	6.05	6.03	6.04	5.92	5.94	5.92	5.92	5.91	5.94
Ti	-	0.01	0.01	0.01	0.13	0.01	0.01	0.01	0.01	0.13
Al	-	-	-	bdl	bdl	-	-	-	-	0.00
Fe	0.03	0.00	bdl	0.01	0.02	-	-	-	-	bdl
Mn	-	bdl	bdl	-	bdl	-	-	-	-	-
Mg	-	-	-	-	bdl	-	-	-	-	-
Ca	-	bdl	bdl	bdl	bdl	-	-	-	-	0.00
Na	0.33	0.15	bdl	bdl	0.00	0.13	0.07	0.08	0.09	0.02
K	1.79	1.79	1.95	1.86	1.92	1.68	1.79	1.80	1.81	1.78
Zr	1.02	0.95	0.98	0.96	0.87	1.10	1.11	1.10	1.10	0.98
Hf	-	-	-	0.02	-	-	-	-	-	-
Ba	-	-	-	-	bdl	-	-	-	-	bdl
P	-	-	-	-	-	-	-	-	-	-
La	-	bdl	bdl	0.00	-	-	-	-	-	-
Ce	-	bdl	bdl	0.00	bdl	-	-	-	-	-
Nb	-	bdl	bdl	-	0.07	-	-	-	-	-
Sum	9.11	8.95	8.97	8.90	8.93	8.86	8.9	8.91	8.92	8.85
K_{alk}	23.27	21.68	21.74	20.9	21.5	20.43	20.9	21.1	21.3	20.34

TABLE 1. (*contd.*)

Location	Murun	Murun	Murun	Murun	Murun	Sunnfjord	Sunnfjord	Sunnfjord	Sunnfjord	Sunnfjord
Group	2	2	2	2	2	2	2	2	2	2
Host rock		Charoitite	Charoitite	Charoitite	Charoitite	Syenite dyke	Syenite dyke	Syenite dyke	Syenite dyke	Syenite dyke
Suggested origin	Magmatic or Metasomatic	Magmatic or Metasomatic	Magmatic or Metasomatic	Magmatic or Metasomatic	Magmatic or Metasomatic	Magmatic	Magmatic	Magmatic	Magmatic	Magmatic
No.	11	12	13	14	15	16	17	18	19	20
SiO_2	60.82	63.44	62.35	61.83	62.25	63.39	61.86	64.94	64.12	64.22
TiO_2	0.69	2.92	5.86	0.69	1.56	0.64	1.22	1.59	0.83	0.88
Al_2O_3	bdl	bdl	0.02	bdl	bdl	0.03	0.01	bdl	0.15	0.06
FeO	bdl	0.01	0.07	bdl	bdl	0.22	0.3	0.26	0.31	0.19
MnO	-	-	-	bdl	bdl	0.05	bdl	0.06	bdl	bdl
MgO	-	-	-	bdl	bdl	bdl	0.08	bdl	bdl	0.05
CaO	0.03	bdl	bdl	bdl	bdl	0.04	bdl	0.03	bdl	bdl
Na_2O	0.03	bdl	0.10	bdl	bdl	0.04	bdl	0.09	bdl	bdl
K_2O	15.41	16.75	16.68	15.15	15.65	15.93	16.64	14.08	15.80	16.36
ZrO_2	22.16	16.68	14.84	20.60	19.13	19.49	18.83	19.13	20.17	19.68
HfO_2	-	-	-	bdl	bdl	-	-	-	-	-
BaO	bdl	bdl	bdl	bdl	bdl	0.08	0.03	0.11	0.04	0.03
P_2O_5	-	-	-	bdl	bdl	0.10	0.12	bdl	bdl	bdl
La_2O_3	-	-	-	bdl	bdl	-	-	-	-	-
Ce_2O_3	-	-	-	bdl	bdl	-	-	-	-	-
Nb_2O_5	-	-	-	bdl	0.60	-	-	-	-	-
Total	99.14	99.79	99.92	98.27	99.19	100.01	99.09	100.29	101.42	101.47
Si	5.92	6.01	5.89	6.00	5.98	6.04	5.98	6.08	6.02	6.03
Ti	0.05	0.21	0.42	0.05	0.11	0.05	0.09	0.11	0.06	0.06
Al	bdl	bdl	0.00	bdl	bdl	0.00	0.00	bdl	0.02	0.01
Fe	bdl	0.00	0.01	bdl	bdl	0.02	0.02	0.02	0.02	0.01
Mn	-	-	-	bdl	bdl	0.00	bdl	0.00	bdl	bdl
Mg	-	-	-	bdl	bdl	bdl	0.01	bdl	bdl	0.01
Ca	0.00	bdl	-	bdl	bdl	0.00	bdl	0.00	bdl	bdl
Na	0.01	bdl	0.02	bdl	bdl	0.01	bdl	0.02	bdl	bdl
K	1.91	2.03	2.01	1.88	1.92	1.94	2.05	1.68	1.89	1.96
Zr	1.05	0.77	0.68	0.98	0.9	0.91	0.89	0.87	0.92	0.9
Hf	-	-	-	bdl	bdl	-	-	-	-	-
Ba	bdl	bdl	bdl	bdl	bdl	0.00	0.00	0.00	0.00	0.00
P	-	-	-	bdl	bdl	0.01	0.01	bdl	bdl	bdl
La	-	-	-	bdl	bdl	-	-	-	-	-
Ce	-	-	-	bdl	bdl	-	-	-	-	-
Nb	-	-	-	bdl	0.03	-	-	-	-	-
Sum	8.94	9.02	9.03	8.91	8.93	8.97	9.05	8.79	8.94	8.98
K_{alk}	21.48	22.51	22.48	21.07	21.47	21.71	22.65	19.34	21.16	21.8

TABLE 1. (*contd.*)

Location	Sunnfjord	Sunnfjord	Sunnfjord	Sunnfjord	Sunnfjord	Cancarix	Cancarix	Cancarix	Cancarix	Cancarix	Cancarix
Group	2	2	2	2	2	2	2	2	2	2	2
Host rock	Syenite dyke	Syenite dyke	Syenite dyke	Syenite dyke	Syenite dyke	Lamproite	Lamproite	Lamproite	Lamproite	Lamproite	Lamproite
Suggested origin	Magmatic	Magmatic	Magmatic	Magmatic	Magmatic	Magmatic	Magmatic	Magmatic	Magmatic	Magmatic	Magmatic
No.	21	22	23	24	25	26	27	28	29	30	31
SiO_2	62.75	62.25	62.53	62.58	62.04	62.60	62.45	62.65	62.95	62.65	63.00
TiO_2	1.08	1.54	1.21	1.61	1.71	1.25	1.10	1.10	0.75	1.15	0.85
Al_2O_3	0.01	0.13	0.12	0.07	0.03	0.10	0.10	0.10	0.05	0.05	0.05
FeO	0.60	0.31	0.19	0.15	0.28	0.18	0.18	0.18	0.18	0.09	0.18
MnO	0.04	0.05	bdl	bdl	0.03	bdl	-	-	-	-	-
MgO	0.65	0.10	0.08	0.02	0.06	bdl	bdl	-	0.05	bdl	0.05
CaO	0.04	0.04	0.06	bdl	0.02	bdl	-	-	-	-	-
Na_2O	bdl	0.19	bdl	bdl	0.07	0.15	0.15	0.15	0.10	0.15	0.15
K_2O	15.79	15.33	15.98	16.17	13.93	15.75	16.10	16.10	15.95	16.25	16.10
ZrO_2	18.29	19.22	18.46	20.23	20.16	19.10	19.20	19.35	19.40	19.60	19.7
HfO_2	-	-	-	-	-	-	-	-	-	-	-
BaO	bdl	0.19	0.21	0.20	0.22	0.45	0.30	0.40	0.15	0.25	0.35
P_2O_5	0.04	0.10	bdl	bdl	bdl	-	-	-	-	-	-
La_2O_3	-	-	-	-	-	-	-	-	-	-	-
Ce_2O_3	-	-	-	-	-	-	-	-	-	-	-
Nb_2O_5	-	-	-	-	-	-	-	-	-	-	-
Total	99.29	99.45	98.84	101.03	98.55	99.58	99.58	100.03	99.58	100.19	100.43
Si	6.01	5.97	6.02	5.94	5.97	6.00	6.00	6.00	6.02	5.99	6.00
Ti	0.08	0.11	0.09	0.11	0.12	0.09	0.08	0.08	0.05	0.09	0.06
Al	0.00	0.01	0.01	0.01	0.00	0.01	0.01	0.01	0.01	0.01	0.01
Fe	0.05	0.02	0.02	0.01	0.02	0.02	0.02	0.02	0.02	0.02	0.02
Mn	0.00	0.00	bdl	bdl	0.00	bdl	-	-	-	-	-
Mg	0.09	0.01	0.01	0.00	0.01	bdl	bdl	-	0.01	bdl	0.01
Ca	0.00	0.00	0.01	bdl	0.00	bdl	-	-	-	-	-
Na	bdl	0.04	bdl	bdl	0.01	0.03	0.03	0.03	0.02	0.03	0.03
K	1.93	1.87	1.96	1.96	1.71	1.93	1.97	1.97	1.95	1.99	1.96
Zr	0.85	0.90	0.87	0.94	0.95	0.90	0.90	0.91	0.91	0.91	0.91
Hf	-	-	-	-	-	-	-	-	-	-	-
Ba	bdl	0.01	0.01	0.01	0.01	0.02	0.01	0.02	0.01	0.01	0.01
P	0.00	0.01	0.00	bdl	bdl	-	-	-	-	-	-
La	-	-	-	-	-	-	-	-	-	-	-
Ce	-	-	-	-	-	-	-	-	-	-	-
Nb	-	-	-	-	-	-	-	-	-	-	-
Sum	9.02	8.96	9.00	8.98	8.82	8.99	9.02	9.01	8.99	9.02	9.01
K_{alk}	21.42	21.29	21.78	21.8	19.55	21.83	22.2	22.17	21.89	22.28	22.06

Analyses 1–2 from Ascension Island, (van Tassel, 1952; Harris and Rickard, 1987), analysis 3 from Straumsvola, Antarctica (Harris and Rickard, 1987), analysis 4 from the Strange Lake complex, Canada (Birkett *et al*., 1992), analysis 5 from Gordon Butte, USA (Chakhmouradian and Mitchell, 2002), analyses 6–9 from Agua de Pau, São Miguel Island (Ridolfi *et al*., 2003), analyses 10–15 from the Murun complex, Russia (Lazebnik and Makhotko, 1982; Konev *et al*., 1996; Reguir, 2001), analyses 16–25 from Sunnfjord, Norway (Robins *et al*., 1983), analyses 26–31 from Cancarix, Spain (Linthout *et al*., 1988). Abbreviations and symbols used: (-) = not analysed; † analysis includes 0.64 wt.% H_2O; * average of three analyses; bdl = below detection limit. K_{alk} calculated after Khomyakov (1995). All structural formulae recalculated from reported weight percent oxide values.

TABLE 2. Average detection limits and errors for Terceira dalyite composition.

	Detection limit (wt.%)	Oxide error (wt.%)	Formula error (apfu)
SiO_2	0.034	0.326	0.045
TiO_2	0.038	0.054	0.004
Al_2O_3	0.020	0.027	0.003
Cr_2O_3	0.023	bdl	bdl
FeO	0.038	0.052	0.004
MnO	0.022	0.030	0.002
MgO	0.020	0.024	0.003
CaO	0.024	bdl	bdl
Na_2O	0.046	0.078	0.015
K_2O	0.021	0.199	0.026
ZrO_2	0.062	0.524	0.025
HfO_2	0.032	0.055	0.002
BaO	0.045	0.073	0.003
Total		0.661	

bdl = values below detection limit.

Mg). This was undertaken using the *GULP* code (Gale, 1997). This code uses effective interatomic potentials to model the interactions between atoms, and has been widely used to calculate the structure and properties of inorganic materials. The Buckingham potential, supplemented by an electrostatic term, is used:

$$V(r) = A\exp(-r/p) - Cr^{-6} + q_1q_2/r \quad (1)$$

In this equation, the adjustable parameters A, ρ and C are fitted to structures and properties of related materials; here they have been transferred from studies on zircon (Akhtar and Waseem, 2001). The charges of the interacting ions are q_1 and q_2; the interatomic distance is r. The experimental and calculated lattice parameters for dalyite are given in Table 3 below, using the experimental structure from Fleet (1965) for comparison. It is seen that the lattice parameters agree to within a few percent, which gives confidence in using this transferred potential. The calculations reported here have been used to obtain the energies involved when various ions are substituted into the dalyite lattice. The calculation of substitutional and solution energies for dopant ions in materials has been widely described elsewhere; see, for example, a recent study of Nd, Gd and Yb ions in BaF_2 (Mujaji *et al.*, 2014). However, a brief summary will be given here. In the case of the substitution of Ti^{4+} into the dalyite lattice, the following reaction (solution scheme) is considered, assuming substitution at the Zr^{4+} site:

$$TiO_2 + Zr_{Zr} \rightarrow Ti_{Zr} + ZrO_2.$$

The energy of this reaction (the solution energy), E_{sol}, is then calculated, as follows:

$$E_{sol} = [E_{latt}(ZrO_2) + E(Ti_{Zr})] - E_{latt}(TiO_2) \quad (2)$$

where E_{latt} is the calculated lattice energy. In this case no charge compensation is needed, but considering substitution at the K^+ site, the following scheme was assumed (with charge compensation by K^+ vacancies):

$$TiO_2 + 4K_K^{\bullet\bullet\bullet} \rightarrow Ti_K + 3V_K' + 2K_2O$$

TABLE 3. Comparison of experimental and calculated lattice parameters.

Lattice parameter	Experimental	Calculated	% Difference
a/Å	7.371	7.211	–2.17
b/Å	7.730	7.679	–0.66
c/Å	6.912	6.787	–1.80
β/degrees	106.23	104.82	–1.33

https://doi.org/10.1180/minmag.2016.080.018 Published online by Cambridge University Press

The solution energy for this reaction is:

$$E_{sol} = [E(Ti_K^{\bullet\bullet\bullet}) + 3E(V'_K) + 2E_{latt}(K_2O)] - E_{latt}(TiO_2) \quad (3)$$

In each case, a similar procedure is adopted, and a single solution scheme is assumed. More complex solution schemes, such as coupled substitutions, cannot be ruled out. Note that in the above expressions, Kröger-Vink notation has been used (Kröger and Vink, 1956).

Results

Petrography of the Caldeira-Castelinho Ignimbrite ejecta

Mineral assemblages of the CCI syenite ejecta include sodic alkali-feldspar, Na-pyroxene, Na-Ca to Na amphibole, quartz, aenigmatite and fayalite with accessory Ti-magnetite, ilmenite, apatite, dalyite, an unspecified eudialyte-group phase and biotite. Significant grain-size variation exists between nodules, allowing the broad distinction of two groups; fine- to medium- (~0.5 to 1.5 mm) grained nodules (Fig. 2*a*), and medium- to coarse- (~1.0 to 6.0 mm) grained nodules (Fig. 2*b*). Typically, the fresher samples are more friable, whereas the more altered samples appear more indurated. Some samples exhibit patches of granular texture, comprising predominantly alkali-feldspar and quartz of finer grain size than the surrounding material. Rarely, samples exhibit mineral modal and/or grain size layering at the cm-scale.

Alkali-feldspar is by far the most abundant phase in all of the nodules and ranges from fresh and unaltered crystals, to heavily altered, perthitic crystals. Pyroxenes and amphiboles are the dominant intercumulus phases. Quartz is also an intercumulus phase and is generally found as large rounded grains or aggregates. Aenigmatite is typically present in small amounts and often exhibits a complex reaction relationship with pyroxene, amphibole and Fe-Ti oxides. When not associated with the apparent breakdown of aenigmatite, Fe-Ti oxides are usually observed as inclusions within other phases (primarily alkali-feldspar). Apatite exists as small, acicular inclusions within alkali-feldspars and varies in abundance between samples. Dalyite is typically present as small (<0.5 mm) sub- to anhedral crystals (Fig. 2*c–e*), though can reach sizes of 1 to 1.5 mm (Fig. 2*f*). It is almost exclusively anhedral and confined to the interstices, either filling or partially filling void spaces. It is often associated spatially with quartz, and in some cases can be found as inclusions within larger interstitial quartz crystals. An unspecified eudialyte-group mineral is found rarely as frequently zoned anhedral crystals that, like dalyite, appear to totally or partially infill interstitial pore spaces, and are often spatially associated with clinopyroxene. Biotite is uncommon and, where present, exists as small inclusions within alkali-feldspars.

Whole-rock and mineral compositions

Whole rock

The results of four whole-rock major-element analyses of dalyite-bearing syenite nodules are given in Table 4. Major-element compositions are relatively uniform, with the variation of individual elements generally being restricted to <1 wt.%. Peralkalinity indices and Na_2O/K_2O ratios range from 1.08 to 1.14 and 1.42 to 1.51, respectively. Calculated CIPW norms yield quartz, albite, orthoclase, diopside, hypersthene, acmite, ilmenite, apatite and sodium metasilicate. All samples are silica-oversaturated, with between 1.0 and 3.3 wt.% normative quartz.

Dalyite chemistry

The results of new chemical analyses of the CCI syenite dalyite (samples TER 30-1 and TER 30-7) are reported in Table 5. The data reveal that the CCI syenite dalyite does not deviate substantially from the empirical formula, with Na being the most significant substituting element (~0.10 to 0.20 atoms per formula unit, apfu), substituting for K. The combined totals of atomic Na and K are close to the ideal total of 2 cations, and Fe contents are often below the detection limit (0.038 wt.%, average error = 0.052 wt.%), highlighting limited incorporation of Fe in the dalyite structure. The low contents of Ti and Hf (up to 0.030 and 0.013 apfu, respectively), indicate that replacement of Zr with Ti and Hf is limited. These data suggest that the CCI dalyite corresponds to the more precise formula $(K_{1.79–1.87}Na_{0.12–0.19})(Zr_{0.90–0.96}Ti_{0.004–0.030}\ Hf_{0.010–0.013})(Si_{6.01–6.06}O_{15})$. Calculated alkalinity moduli (Khomyakov, 1995) values range from 21.90 to 22.39. In addition to Na, Fe Ti and Hf, the data suggest that trace amounts of Al, Ba, Mg, and Mn may be present, though these are all very close to the detection limit. This is supported by their

https://doi.org/10.1180/minmag.2016.080.018 Published online by Cambridge University Press

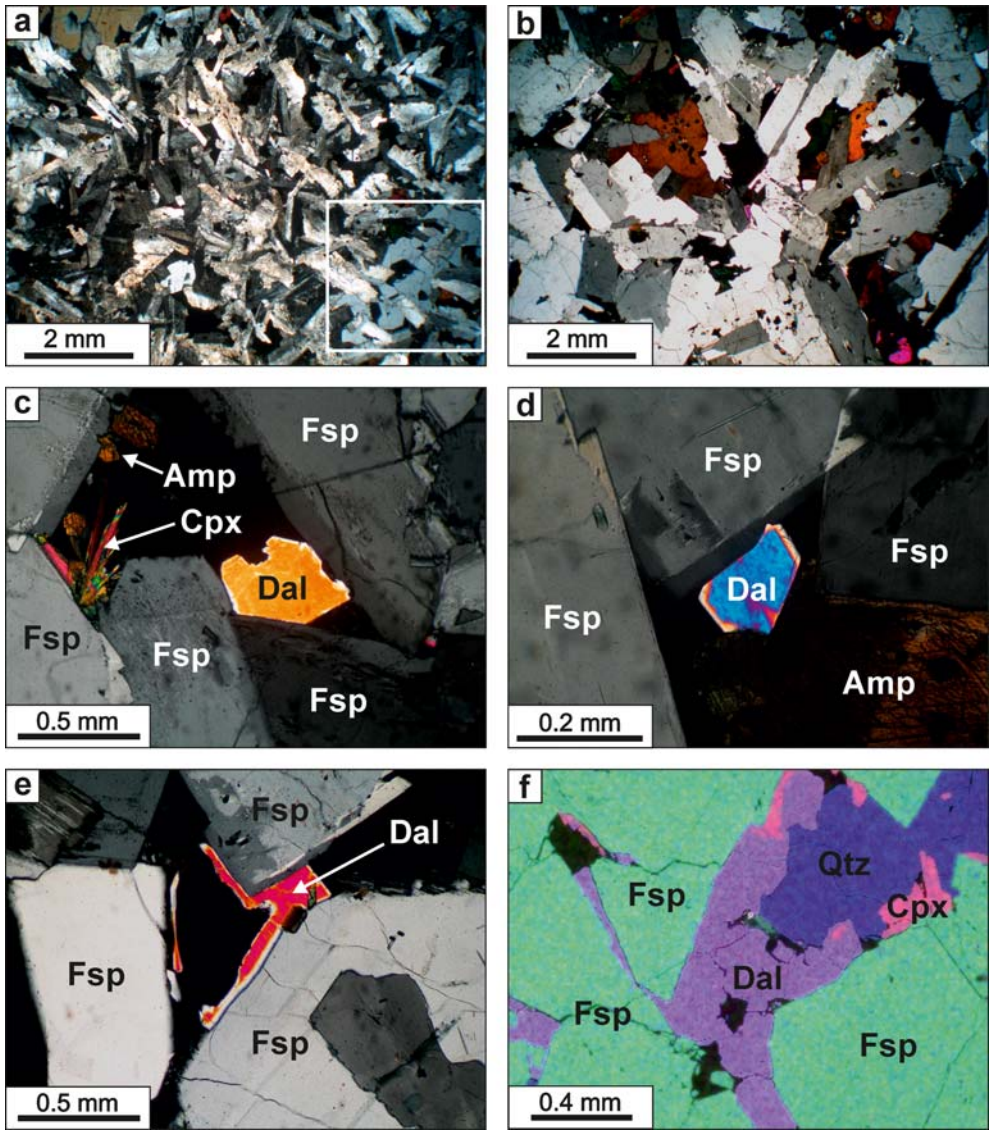

FIG. 2. (*a*) Example of a fine- to medium-grained alkali-feldspar dominated nodule. The feldspars appear altered and are often perthitic. A large, optically-continuous quartz crystal is highlighted with a white box in the lower right corner of the image. (*b*) A medium- to coarse-grained nodule with larger crystal sizes and fresher, less-altered feldspars. (*c*) A large dalyite crystal which partially infills an interstitial void between larger alkali-feldspar crystals. Also visible are small amphibole crystals and stellate clinopyroxene. (*d*) An anhedral dalyite crystal which partially fills an interstitial void between large alkali-feldspars and a large amphibole crystal. (*e*) An anhedral dalyite crystal forming an incomplete rim around the edges of an interstitial cavity. A small clinopyroxene crystal appears to have been included within the dalyite. A resorbed, optically distinctive feldspar core is visible within the large feldspar to the lower right of the image. (*f*) An element map highlighting a large, anhedral dalyite crystal filling an interstitial space, together with intergrown quartz and small amounts of clinopyroxene. Colours used: Red = Fe, Purple = Zr, Blue = Si, Green = Al. Abbreviations used: Qtz = quartz, Fsp = alkali-feldspar, Amp = amphibole, Cpx = clinopyroxene, Dal = dalyite.

https://doi.org/10.1180/minmag.2016.080.018 Published online by Cambridge University Press

TABLE 4. Whole-rock major-element analyses of the CCI syenite ejecta.

Sample	TER 30-1	TER 35-1	TER 30-6	TER 30-7
SiO_2	64.14	64.78	63.90	64.80
TiO_2	0.58	0.45	0.61	0.41
Al_2O_3	15.76	15.51	15.82	16.18
Fe_2O_3	5.34	5.29	5.57	4.53
MnO	0.21	0.20	0.22	0.17
MgO	0.36	0.27	0.36	0.27
CaO	0.82	0.44	0.76	0.54
Na_2O	7.44	7.41	7.36	7.25
K_2O	4.93	5.11	4.98	5.10
P_2O_5	0.08	0.06	0.07	0.05
LOI	0.10	0.30	0.10	0.40
Total	99.76	99.82	99.75	99.70
A.I.	1.12	1.14	1.11	1.08
Na_2O/K_2O	1.51	1.45	1.48	1.42
CIPW				
Q	1.52	3.33	1.00	2.42
Or	29.25	30.32	29.55	30.14
Ab	53.76	51.58	53.84	54.83
An	0.00	0.00	0.00	0.00
Di	3.08	1.57	2.88	2.06
Hy	4.40	5.05	4.54	5.55
Ac	6.02	5.64	6.10	2.05
Il	1.10	0.85	1.16	0.78
Ap	0.19	0.14	0.16	0.12
NaS	0.61	1.18	0.41	0.97

occurrence in trace amounts in various literature data (Table 1).

Solid-state modelling

Calculated solution energies (E_{sol}) for a number of potential substitutions are presented in Table 6. In each instance, the lowest E_{sol} value is considered to highlight the most likely substitution. Model results for Ti indicate Ti↔Si substitution as the most energetically favourable (E_{sol} = –0.98 eV), though Ti↔Zr substitution is also likely (E_{sol} = –0.25 eV). Modelling of Hf is more conclusive, with Hf↔Zr substitution representing the most likely scenario (E_{sol} = –0.31 eV). The incorporation of the R^{2+} cations Fe^{2+}, Mg^{2+} and Ba^{2+} was also modelled, but charge balancing necessitates the presence of site vacancies, in this case assumed to be a single O vacancy. Results indicate that, in the case of Fe^{2+} and Mg^{2+} the lowest energy scenario is replacement of K. Nevertheless, the calculated E_{sol} values of 8.86 eV and 9.61 eV, respectively, highlight the overall difficulty of their inclusion within the dalyite structure. Modelling of Ba yields a similar result, though the calculated E_{sol} value of 4.94 eV for Ba↔K substitution is noticeably lower than other R^{2+} cations.

Discussion

Variations in dalyite chemical composition

To facilitate a wider discussion of the compositional variability of dalyite, all available analyses are divided into two groups: (1) dalyite found within peralkaline syenitic or granitic rocks, and (2) dalyite found within other lithologies, including lamproites, lamprophyres and charoitites. As such, the dalyite analyses of samples from Terceira, São Miguel, Ascension, Straumsvola, Strange Lake and Gordon Butte are included in Group 1, whereas analyses of Sunnfjord, Murun and Cancarix samples occupy Group 2. All analyses were tested for quality using the following criteria: (i) analysis total = 100 wt.% ± 1.5, (ii) total cations = <9.05 apfu, (iii) cation total for the tetrahedral site = 6 apfu ± 0.05, (iv) cation total for the octahedral site = 1 apfu ± 0.05. Only

https://doi.org/10.1180/minmag.2016.080.018 Published online by Cambridge University Press

TABLE 5. Electron-microprobe analyses of dalyite from CCI syenite ejecta. Oxides reported as wt.%, structural formulas calculated on the basis of 15 oxygens.

Sample	TER 30-1	TER 30-1	TER 30-1	TER 30-1	TER 30-1	TER 30-7	TER 30-7	TER 30-7	TER 30-7	TER 30-7	TER 30-7	TER 30-7
Group	1	1	1	1	1	1	1	1	1	1	1	1
Suggested origin	Magmatic	Magmatic	Magmatic	Magmatic	Magmatic	Magmatic	Magmatic	Magmatic	Magmatic	Magmatic	Magmatic	Magmatic
SiO_2	62.9	62.6	62.4	62.2	62.4	62.9	63.0	62.4	62.6	62.6	63.0	63.0
TiO_2	0.10	0.23	0.19	0.13	0.11	0.17	0.10	0.12	0.41	0.09	0.06	0.27
Al_2O_3	bdl	bdl	0.03	0.03	bdl	bdl	0.04	0.04	0.05	0.03	bdl	bdl
Cr_2O_3	bdl	bdl	bdl	bdl	bdl	bdl	bdl	bdl	bdl	bdl	bdl	bdl
FeO	bdl	0.06	bdl	0.06	0.09	bdl	0.07	0.07	0.11	0.05	0.06	bdl
MnO	bdl	0.03	bdl	bdl	bdl	bdl	bdl	0.04	bdl	bdl	bdl	bdl
MgO	bdl	bdl	bdl	bdl	bdl	bdl	bdl	bdl	0.03	bdl	bdl	bdl
CaO	bdl	bdl	bdl	bdl	bdl	bdl	bdl	bdl	bdl	bdl	bdl	bdl
Na_2O	0.99	0.95	0.99	1.00	0.90	0.90	0.67	0.71	0.67	0.72	0.66	0.66
K_2O	14.6	15.0	14.9	14.8	14.7	14.8	15.0	15.0	15.0	15.2	15.3	15.1
ZrO_2	20.0	20.5	19.8	20.4	20.4	20.4	19.7	20.3	19.1	20.0	20.6	20.2
HfO_2	0.46	0.40	0.38	0.40	0.39	0.45	0.39	0.39	0.42	0.42	0.48	0.38
BaO	0.06	0.06	0.08	bdl	bdl	0.05	0.08	bdl	bdl	bdl	bdl	bdl
Total	99.08	99.78	98.81	98.89	98.98	99.72	98.99	99.05	98.33	99.01	100.17	99.57
Si	6.05	6.01	6.03	6.01	6.02	6.03	6.06	6.02	6.05	6.04	6.02	6.04
Ti	0.007	0.016	0.013	0.009	0.008	0.012	0.008	0.009	0.030	0.006	0.004	0.019
Al	bdl	bdl	0.004	0.003	bdl	bdl	0.005	0.004	0.006	0.004	bdl	bdl
Cr	bdl	bdl	bdl	bdl	bdl	bdl	bdl	bdl	bdl	bdl	bdl	bdl
Fe	bdl	0.005	bdl	0.004	0.007	bdl	0.005	0.006	0.009	0.004	0.005	bdl
Mn	bdl	0.002	bdl	bdl	bdl	bdl	bdl	0.004	bdl	bdl	bdl	bdl
Mg	bdl	bdl	bdl	bdl	bdl	bdl	bdl	bdl	0.004	bdl	bdl	bdl
Ca	bdl	bdl	bdl	bdl	bdl	bdl	bdl	bdl	bdl	bdl	bdl	bdl
Na	0.18	0.18	0.18	0.19	0.17	0.17	0.13	0.13	0.13	0.13	0.12	0.12
K	1.79	1.84	1.83	1.82	1.81	1.81	1.84	1.85	1.85	1.87	1.87	1.85
Zr	0.94	0.96	0.93	0.96	0.96	0.95	0.92	0.96	0.90	0.94	0.96	0.94
Hf	0.013	0.011	0.010	0.011	0.011	0.012	0.011	0.011	0.011	0.012	0.013	0.010
Ba	0.002	0.002	0.003	bdl	bdl	0.002	0.003	bdl	bdl	bdl	bdl	bdl
Sum	8.982	9.026	9.000	9.007	8.986	8.986	8.982	8.994	8.990	9.006	8.992	8.979
K_{alk}	21.98	22.34	22.39	22.32	22.06	21.99	21.90	22.03	21.98	22.27	22.13	21.94

TABLE 6. Results of computer modelling undertaken using the *GULP* code (Gale, 1997).

Substitution	Solution scheme	E_{sol} (eV)
Ti → Zr	$TiO_2 + Zr_{Zr} \rightarrow Ti_{Zr} + ZrO_2$	–0.25
Ti → Si	$TiO_2 + Si_{Si} \rightarrow Ti_{Si} + SiO_2$	–0.98
Ti → K	$TiO_2 + 4K_K \rightarrow Ti_K^{\bullet\bullet\bullet} + 3V_K' + 2K_2O$	30.64
Hf → Zr	$HfO_2 + Zr_{Zr} \rightarrow Hf_{Zr} + ZrO_2$	–0.31
Hf → Si	$HfO_2 + Si_{Si} \rightarrow Hf_{Si} + SiO_2$	2.67
Hf → K	$HfO_2 + 4K_K \rightarrow Hf_K^{\bullet\bullet\bullet} + 3V_K' + 2K_2O$	29.09
Fe^{2+} → Zr	$FeO + Zr_{Zr} \rightarrow Fe_{Zr}'' + V_O^{\bullet\bullet} + ZrO_2$	12.52
Fe^{2+} → Si	$FeO + Si_{Si} \rightarrow Fe_{Si}'' + V_O^{\bullet\bullet} + SiO_2$	13.69
Fe^{2+} → K	$FeO + K_K \rightarrow Fe_K^{\bullet} + V_K' + K_2O$	8.86
Mg^{2+} → Zr	$MgO + Zr_{Zr} \rightarrow Mg_{Zr}'' + V_O^{\bullet\bullet} + ZrO_2$	12.97
Mg^{2+} → Si	$MgO + Si_{Si} \rightarrow Mg_{Si}'' + V_O^{\bullet\bullet} + SiO_2$	14.07
Mg^{2+} → K	$MgO + K_K \rightarrow Mg_K^{\bullet} + V_K' + K_2O$	9.61
Ba^{2+} → Zr	$BaO + Zr_{Zr} \rightarrow Ba_{Zr}'' + V_O^{\bullet\bullet} + ZrO_2$	12.54
Ba^{2+} → Si	$BaO + Si_{Si} \rightarrow Ba_{Si}'' + V_O^{\bullet\bullet} + SiO_2$	16.58
Ba^{2+} → K	$BaO + K_K \rightarrow Ba_K^{\bullet} + V_K' + K_2O$	4.94

those analyses which passed all four criteria were applied to the following discussion, reducing the size of the dataset from 43 to 25.

The overall average calculated 'alkalinity modulus', K_{alk} (Khomyakov, 1995) for the combined dataset is 21.94, with minimum and maximum values of 20.90 and 22.51, respectively. This shows essentially no variation between Groups 1 and 2, with average values of 21.98 and 21.91, respectively.

The available dalyite analytical data in K–Na space are shown in Fig. 3*a*. The data typically lie within 0.05 apfu of the one-to-one line, indicating the role of one-to-one K↔Na substitution within the polyhedral sites. Group 1 analyses are characterized by a relative abundance of Na (0.12 to 0.19 apfu) and a corresponding paucity of K (1.79 to 1.87 apfu), though two analyses from Straumsvola and Strange Lake (analyses 3 and 4, Table 1) exhibit Na concentrations below the detection limit, alongside a slight deficiency in K. This discrepancy in older dalyite analyses may indicate Na loss during analysis, as suggested by Birkett *et al.* (1992). The dalyite from Strange Lake may also have been subject to alteration, as it is described as being frequently rimmed by elpidite or vlasovite.

In contrast to Group 1, Group 2 analyses are closer to the ideal dalyite formula, with significantly lower concentrations of Na (<0.015 to 0.03 apfu). The relatively sodic nature of group 1 and potassic nature of Group 2 dalyite correlates with the relatively sodic nature of the Group 1 rocks and the generally potassic nature of Group 2 rocks. For example, reported whole rock Na_2O/K_2O ratios of Group 1 typically lie between 1 and 1.5 (Harris and Rickard, 1987; Ridolfi *et al.*, 2003; this study). In contrast, Group 2 whole rock Na_2O/K_2O is likely to be significantly lower, given their often highly potassic nature, as is the case for the Cancarix dalyite (Na_2O/K_2O = 0.1, Linthout *et al.*, 1988; Salvioli-Mariani and Venturelli, 1996). Harris and Rickard (1987) made a similar observation, noting that the dalyite analyses from Sunnfjord (analyses 16 to 25, Table 1) exhibit lower Na contents than dalyite from Ascension Island (analysis 2, Table 1), which they attributed to the higher Na_2O/K_2O ratio of the latter. However, they also noted that Straumsvola dalyite (analysis 3, Table 1) has essentially no Na, despite a highly comparable Na_2O/K_2O ratio to that of Group 1 samples (1.35).

Another potential control that must be considered is the crystallization mechanism of each example, which must also play a role in the composition of dalyite. For example, the dalyite-bearing, ultrapotassic Sunnfjord dyke is reported to be heavily hydrothermally altered (Furnes *et al.*, 1982), suggesting that any dalyite present may be metasomatic in origin, or a magmatic composition that has been altered by metasomatism. It can be seen in Table 1 that those analytical data that may have been influenced by metasomatism (e.g. Sunnfjord, Murun) frequently exhibit Na contents below detection. However, although the Straumsvola

https://doi.org/10.1180/minmag.2016.080.018 Published online by Cambridge University Press

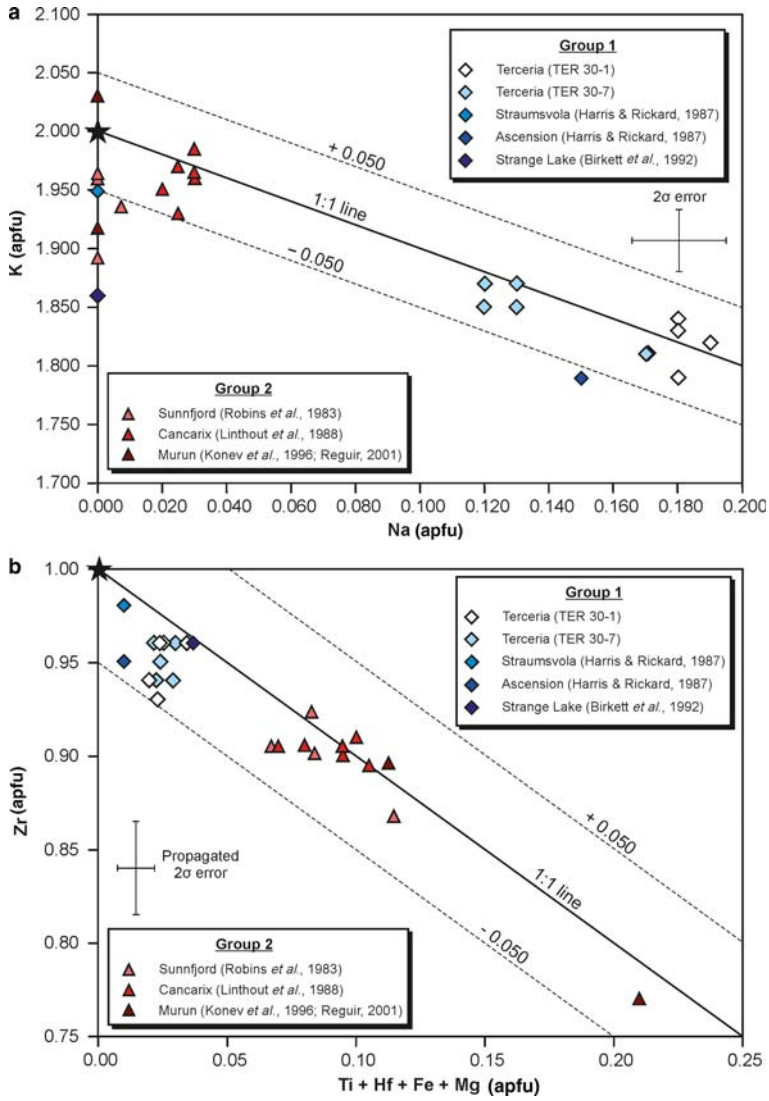

FIG. 3. Geochemical variation diagrams highlighting the variable degree of substitution within the dataset. The ideal composition of dalyite is highlighted with a black star symbol. The maximum error is applicable to the new data for Terceira (TER 30-1 and TER 30-7) only and is calculated as described in the text. Group 1 dalyite is denoted by diamonds, Group 2 by triangles. Only analyses that passed all of the filtering criteria described in the text are shown. (*a*) Bivariate plot showing the degree of K↔Na substitution in the dataset. (*b*) Bivariate plot showing the degree of substitution in the octahedral site. Data for Hf, Mg and Fe is presented where analyses permit.

analysis (itself an average of three analyses) contains no significant Na, the peralkaline granite host rock is described as being very fresh (Harris and Rickard, 1987), and so the reported Na-poor dalyite cannot be attributed entirely to the effects of crystallization mechanism or alteration.

The degree of substitution within the octahedral sites is highlighted in Fig. 3*b*. Titanium and Hf are considered as the most suitable substitutes, though the R^{2+} cations Mg, Mn and Fe are also considered (where data is available), due to the similarity of their ionic radii with Zr. In Fig. 3*b*, the data plot within 0.05 apfu of the one-to-one line, indicating one-to-one cation exchange. In the case of Fe, Mn and Mg, this would introduce a charge imbalance which can be mitigated by a single oxygen vacancy.

https://doi.org/10.1180/minmag.2016.080.018 Published online by Cambridge University Press

Although solid-state modelling suggests that R^{2+}↔K substitution should be energetically favourable, the calculated E_{sol} values are still too large (8.86 eV and 9.61 eV), and the difference in ionic radii too great, to fully justify the placement of R^{2+} cations in the polyhedral sites. The substitutions of Hf↔Zr and Ti↔Zr are both supported by solid-state modelling (E_{sol} = –0.31 eV and –0.25 eV, respectively, though in the latter case, the modelling also indicates the potential of Ti↔Si substitution (E_{sol} = –0.98 eV). However, there is no evidence within the dataset to support such a substitution.

Group 1 data remain close to the ideal dalyite formula, with 0.91 to 0.98 apfu Zr. Group 2 data exhibit a greater degree of substitution, generally clustering between 0.85 and 0.94 apfu Zr, with 0.05 to 0.12 apfu Ti. It is notable that one of the two analyses from the charoitites of the Murun Complex is enriched in the davanite component ($K_2TiSi_6O_{15}$), with 0.21 apfu Ti. This may relate to the unusual nature of their charoititic host rock, which is typically considered to be metasomatic rather than magmatic in origin (e.g. Reguir, 2001 and references therein). This alternative origin may explain the apparent geochemical deviation from the rest of the dataset.

The dataset indicates the presence of small amounts of Ba within Group 2 dalyite. On the basis of solid-state modelling and ionic radii, it is suggested that the most likely mechanism for its inclusion within the dalyite structure is Ba↔K. The resulting charge imbalance could be mitigated by a single vacancy in the polyhedral site, in which case the Ba content may be used as a proxy for the polyhedral vacancies in each analysis (up to 0.02 apfu). This may, in part, account for analyses in which the structural total is less than the ideal 9 apfu. Alternatively, structural deficits may result from the presence of Li. Significant concentrations of Li have been reported in peralkaline rocks and Li enrichment can occur via metasomatic processes (e.g. Borley, 1963; Hawthorne *et al.*, 1996; Brenan *et al.*, 1998; Hawthorne *et al.*, 2001). Although the mechanisms of Li substitution in dalyite are unclear, its inclusion may contribute to the frequently low structural totals observed within the dataset.

The key geochemical parameters required to stabilize dalyite are high μK_2O and high $aSiO_2$ (Marks *et al.*, 2011). For example, an insufficiently high silica activity will lead to the crystallization of wadeite ($K_2ZrSi_3O_9$) in place of dalyite (Marks *et al.*, 2011). Dalyite is therefore limited to silica-saturated to -oversaturated lithologies, although its occurrence in a nepheline-bearing pegmatite from Langesundfjord, Norway (Andersen *et al.*, 2010) appears to contradict this. The additional requirement of high μK_2O is probably due to high K_2O contents in the melts, achieved either by slowly increasing K_2O via fractional crystallization and/or crustal assimilation of potassic rocks in the Group 1 samples, or by producing melts with initially high K_2O values via the more unusual processes suggested to produce ultrapotassic rocks, such as partial melting of metasomatized mantle lithologies, (e.g. Mitchell and Bergman, 1991).

The geochemical variations observed between the Groups of this study are likely to represent major-element variations in the melts themselves. For example, the Group 2 dalyites generally show elevated Ti and Fe contents relative to the Group 1 dalyites, which may relate to the relatively Ti- and Fe-rich whole-rock compositions of lamproites and lamprophyres, particularly when compared to the low Ti contents of Group 1 whole-rock analyses (<0.7 wt.%). Additionally, Group 2 analyses exhibit significantly lower degrees of Na substituting for K, which might be expected given the K_2O-rich nature of their whole-rock analyses.

Dalyite crystallization on Terceira

Dalyite is generally considered to be a late-stage, magmatic mineral phase (e.g. Harris and Rickard, 1987; Ridolfi *et al.*, 2003) that may be altered, either during later magmatic or sub-solidus stages, to minerals such as elpidite, $Na_2ZrSi_6O_{15}{\cdot}3(H_2O)$ (Cann, 1967), catapleiite, $Na_2Zr(Si_3O_9){\cdot}2H_2O$ (Birkett *et al.*, 1992; Chakhmouradian and Mitchell, 2002) and intergrown quartz and zircon (Cann, 1967). Key features of the Terceira dalyite, notably the dominantly anhedral crystal forms, its restricted occurrence in interstitial pore spaces and its lack of inclusion within other mineral phases, all point towards late-stage, post-cumulus, magmatic crystallization, though extension of the crystallization interval into the sub-solidus deuteric stage cannot be ruled out. Evidence for the alteration of primary dalyite compositions is lacking. Its textural association and occasional intergrowth with quartz suggests that the crystallization of these two phases was largely contemporaneous. This conclusion is in agreement with that of Ridolfi *et al.* (2003), who studied similar parageneses in syenite nodules erupted by Agua de Pau volcano, São Miguel, Azores.

The dalyite analyses from Terceira display two clusters in Na–K space (Fig. 3*a*), with one cluster of more sodic compositions (0.17 to 0.19 Na apfu),

https://doi.org/10.1180/minmag.2016.080.018 Published online by Cambridge University Press

and another cluster of more potassic compositions (0.12 to 0.13 Na apfu). The difference between these clusters cannot be entirely accounted for by the calculated two-sigma errors of ±0.015 apfu, and is considered to represent bimodality in the dataset. Both clusters lie within 0.05 apfu of the one-to-one line and, as such, the trend of the data probably highlights the role of varying degrees of one-to-one Na↔K substitution within the Terceira samples. The presence of two subgroups may imply that two separate populations of dalyite are present, either derived from multiple processes that each led to the crystallization of compositionally distinct dalyite, or a single process that is capable of producing a heterogeneous dalyite population. No visible correlation exists between dalyite composition and textural features such as crystal form or size, or the degree to which they infill pores. Instead, the two clusters of dalyite analyses can be related to the two separate samples in which dalyite was analysed (TER-30-1 and TER 30-7), with the most sodic dalyite analyses being from TER 30-1. The compositional variations may therefore reflect random sampling of a syenitic mush in which geochemical heterogeneity is sufficiently large in scale that it yields 'inter-nodule' variations in dalyite composition, whilst 'intra-nodule' variations are more limited. Such heterogeneity may be primary (i.e. derived from original compositional variations in the melt, perhaps originating from multiple magma batches that contributed to a single crystal mush body), or secondary, originating from the variable degree of fluid-feldspar reaction (albitization; e.g. Lee and Parsons, 1997) in the crystal mush during deuteric alteration. The late-stage albitization of the rock would lead to a bulk-rock increase in Na and an enrichment of K in the albitizing fluids. The prevalence of coarse patchy perthitic feldspars in the Terceira syenites provides evidence for the prominent role of albitization in their late-stage evolution. Evidence for primary bulk compositions being the underlying control upon dalyite composition exists in the bimodality of the dataset, with the most sodic dalyites found in the most sodic whole-rock analysis.

However, a single analysis from sample TER 30-7 falls within the cluster of TER 30-1 analyses (Fig. 2*a*, Table 5), indicating that a simple relationship between dalyite chemistry and bulk-rock composition cannot account entirely for the observed variation. As such, alternative processes that might influence the degree of Na↔K substitution are explored. One example that is considered here is the role of variable pore size in the compositional evolution of interstitial melts. Because heterogeneous nucleation is energetically favourable compared to homogenous nucleation, the dominant process that drives the compositional evolution of a melt within a pore under closed system conditions is the crystallization of surrounding cumulus phases, as components that are incompatible in the pore wall minerals become enriched in the residual melt. In the Terceira syenite nodules, alkali-feldspar is the most abundant phase, and surrounds the majority of pore spaces, suggesting that the post-cumulus, heterogeneous nucleation of feldspar onto pore walls will exert the strongest influence upon interstitial melt compositions. Due to its albite-rich composition (~Ab_{64}, average Na/K = 1.67) (A. J. Jeffery, unpublished data), this effect is likely to promote the development of depressed Na/K ratios in the liquid as evolution continues. Petrographic evidence for this process exists in the form of optically distinguishable rims on many of the pore-wall feldspars (e.g. Fig. 2*c*). During the sub-solidus deuteric stage, albitization also contributes to the depression of liquid Na/K ratios via the replacement of alkali feldspar with near end-member albite. Thus, it is suggested that during the late-stage magmatic and sub-solidus deuteric evolution of the syenite, the majority of liquid-filled pores were evolving towards more potassic compositions.

It is proposed that the observed variation in Terceira dalyite composition could be related to the timing of crystallization relative to the evolution of the interstitial melt. The thermodynamics of crystallization in pore spaces has been shown to be fundamentally different compared to a free fluid (Bigg, 1953; Melia and Moffitt, 1964; Putnis *et al.*, 1995; Scherer, 1999). In particular, a fluid confined to a pore space can achieve greater degrees of supersaturation prior to the onset of crystallization compared with an unconfined fluid, thus introducing a nucleation delay that is more substantial in smaller pores (e.g. Putnis and Mauthe, 2001; Holness *et al.*, 2007; Holness and Sawyer, 2008). As such, the dalyite crystals that grew in smaller pores would have nucleated later than those in larger pores, and would record more evolved compositions. Holness and Sawyer (2008) also cited the prevalence of single-grain pseudomorphs in small pores and poly-mineralic aggregate pseudomorphs in larger pores as petrographic evidence for the relative ease of nucleation in larger pores. This feature can also be observed in the CCI syenite, where larger pores are frequently filled with aggregates of late-crystallizing phases such as quartz, clinopyroxene, dalyite and a

https://doi.org/10.1180/minmag.2016.080.018 Published online by Cambridge University Press

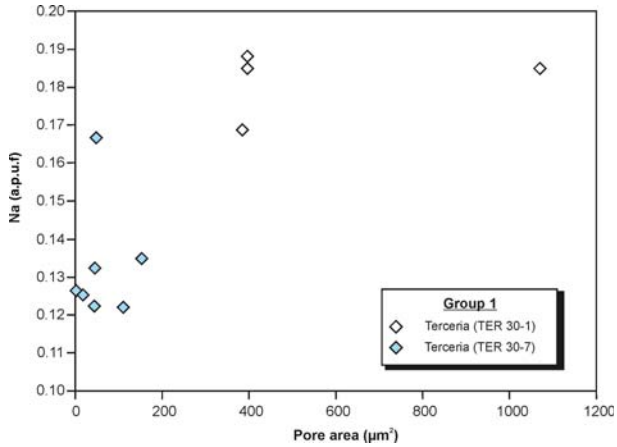

FIG. 4. Bivariate plot of measured pore area against the Na content of dalyite within the pore.

eudialyte-group mineral (Fig. 2*f*), whilst small pores generally contain only a single crystal of one of these phases (Fig. 2*d*).

Considering the previously described evolutionary trend of relative K-enrichment during both late-stage magmatic and sub-solidus stages, dalyite in smaller pores should therefore have more potassic compositions. To test this hypothesis, dalyite-bearing pore spaces were digitized and measured using *ImageJ* to determine the two-dimensional area. This was then plotted against the Na content of the dalyite crystal within them (Fig. 4), yielding a positive correlation that suggests that the size of a pore exerts, at least to some extent, a control over the composition of the dalyite crystallizing within it.

A single data point in Fig. 4 appears to deviate from the broadly linear trend observed in the rest of the data (pore area = 1.07 mm^2, Na content = 0.18). Unlike other reported dalyites, this dalyite crystal is found in a pore that is bounded by a large clinopyroxene crystal, in addition to alkali-feldspar. It is therefore suggested that this deviation in pore size *vs*. Na content space may highlight the influence of other minerals in the evolution of interstitial melts. Given the relatively high Na contents of the Terceira clinopyroxene (~11 to 13 wt.% Na_2O) (Jeffery, 2016), the pore wall crystallization of clinopyroxene would greatly accelerate the described evolutionary trend of K-enrichment in interstitial melt, leading to dalyite compositions that appear unusually K-rich when compared with the suggested feldspar-controlled trend (Fig. 4). The pore wall crystallization of amphibole would also produce this effect but to a lesser degree (~6 wt.% Na_2O) (Jeffery, 2016).

In summary, it is suggested that the dalyite from Terceira is predominantly late-stage magmatic in origin, and the observed compositional variability is influenced by the K-enrichment trend of late-stage interstitial melt resulting from pore wall crystallization of sodic alkali feldspar. Any continued crystallization during a sub-solidus deuteric stage is considered to have been subject to a similar K-enrichment trend, driven by albitization of alkali feldspar. Variation in Na content is likely to have been controlled, at least in part, by the larger nucleation delay that is introduced in smaller pores compared to larger ones.

Conclusions

A new occurrence of the rare potassium zirconium silicate dalyite is reported from Terceira, Azores. The detailed study of new quantitative analyses of dalyite from Terceira, alongside solid-state modelling and previously published analyses, allows the following conclusions to be made regarding the compositional variability of dalyite: (1) Substitution of Na for K in dalyite is generally more significant in peralkaline granites and syenites than in highly potassic rock types. (2) The incorporation of small amounts of Ba occurs in potassic rocks and is most probably achieved via Ba↔K substitution. (3) The incorporation of Fe into dalyite is minimal in peralkaline granites and syenites, but becomes more significant in highly potassic lithologies. Mineral chemical data and solid-state modelling suggest that this is most easily achieved via Fe^{2+}↔Zr substitution, though high

https://doi.org/10.1180/minmag.2016.080.018 Published online by Cambridge University Press

E_{sol} values and charge-balancing requirements must hinder this relationship. (4) The degree of substitution of Ti for Zr is greater in highly potassic igneous rocks than in peralkaline granites and syenites, and may be linked to elevated Ti-contents of the melts. (5) Dalyite from Terceira shows variation in the degree of Na↔K substitution that does not relate obviously to texture, and cannot be entirely attributed to 'inter-nodule' diversity. This feature is linked to relative K-enrichment induced by the effects of pore wall crystallization (during a late-stage magmatic phase) and albitization (during a sub-solidus deuteric phase), coupled with the variation in nucleation delay that is introduced by variable pore sizes.

Acknowledgements

The authors gratefully acknowledge S. Self, A. Pimentel, J. Pacheco and the Centro de Vulcanologia e Avaliação de Riscos Geológicos (CVARG) for their invaluable assistance and logistical support during fieldwork. They are grateful to P. Williams and R. Mitchell for editorial handling and F. Ridolfi and G. Gatta for their detailed and constructive comments, which greatly improved the manuscript. E. Reguir is thanked for providing a copy of Table 48 from Konev *et al.* (1996).

References

Akhtar, M.J. and Waseem, S. (2001) Atomistic simulation studies of zircon. *Chemical Physics*, **274**, 109–120.

Andersen, T., Erambert, M., Larsen, A.O. and Selbekk, R. S. (2010) Petrology of nepheline syenite pegmatites in the Oslo Rift, Norway: zirconium silicate mineral assemblages as indicators of alkalinity and volatile fugacity in mildly agpaitic magma. *Journal of Petrology*, **51**, 2303–2325.

Armstrong, J.T. (1995) CITZAF: a package of correction programs for the quantitative electron microbeam X-ray analysis of thick polished materials, thin films, and particles. *Microbeam Analysis*, **4**, 177–200.

Bigg, E.K. (1953) The supercooling of water. *Proceedings of the Physical Society (London)*, **66B**, 688–694.

Birkett, T.C., Miller, R.R., Roberts, A.C. and Mariano, A.N. (1992) Zirconium-bearing minerals of the Strange Lake Intrusive Complex, Quebec-Labrador. *The Canadian Mineralogist*, **30**, 191–205.

Borley, G.D. (1963) Amphiboles from the Younger Granites of Nigeria. I. Chemical classification. *Mineralogical Magazine*, **33**, 358–376.

Brenan, J.M., Neroda, E., Lundstrom, C.C., Shaw, H.F., Ryerson, F.J. and Phinney, D.L. (1998) Behaviour of boron, beryllium, and lithium during melting and crystallization: constraints from mineral-melt partitioning experiments. *Geochimica et Cosmochimica Acta*, **62**, 2129–2141.

Brod, J.A. (1999) *Petrology and geochemistry of the Tapira alkaline complex, Minas Gerais state, Brazil.* PhD thesis, Durham University, UK, 486 pp.

Cann, J.R. (1967) A second occurrence of dalyite and the petrology of some ejected syenite blocks from São Miguel, Azores. *Mineralogical Magazine*, **36**, 227–232.

Chakhmouradian, A.R. and Mitchell, R.H. (2002) The mineralogy of Ba- and Zr-rich alkaline pegmatites from Gordon Butte, Crazy Mountains (Montana, USA): comparisons between potassic and sodic agpaitic pegmatites. *Contributions to Mineralogy and Petrology*, **143**, 93–114.

Dolivo-Dobrovol'skiy, D.V. and Yevdokimov, M.D. (1991) Zirconium mineralisation of the alkali metasomatites of the Murun Complex. *International Geology Review*, **33**, 490–496.

Fleet, S.G. (1965) The crystal structure of dalyite. *Zeitschrift für Kristallographie*, **121**, 349–368.

Furnes, H., Mitchell, J.G., Robins, B., Ryan, P. and Skjerlie, F.J. (1982) Petrography and geochemistry of peralkaline, ultrapotassic syenite dykes of Middle Permian age, Sunnfjord, West Norway. *Norsk Geologisk Tidsskrift*, **62**, 147–159.

Gale, J.D. (1997) GULP: A computer program for the symmetry-adapted simulation of solids. *Journal of the Chemical Society, Faraday Transactions*, **93**, 629–637.

Gente, P., Dyment, J., Maia, M. and Goslin, J. (2003) Interaction between the Mid-Atlantic Ridge and the Azores hot spot during the last 85 Myr: emplacement and rifting of the hotspot derived plateaus. *Geochemistry, Geophysics, Geosystems*, **4**, doi: 10.1029/2003GC000527.

Gertisser, R., Self, S., Gaspar, J.L., Kelley, S.P., Pimentel, A., Eikenberg, J., Barry, T.L., Pacheco, J.M., Queiroz, G. and Vespa, M. (2010) Ignimbrite stratigraphy and chronology on Terceira Island, Azores. *The Geological Society of America, Special Paper*, **464**, 133–154.

Harris, C. and Rickard, R.S. (1987) Rare-earth-rich eudialyte and dalyite from a peralkaline granite dyke at Straumsvola, Dronning Maud Land, Antarctica. *The Canadian Mineralogist*, **25**, 755–762.

Harris, C., Cressey, G., Bell, J.D., Atkins, F.B. and Beswetherick, S. (1982) An occurrence of rare-earth-rich eudialyte from Ascension Island, South Atlantic. *Mineralogical Magazine,* **46,** 421–425.

Hawthorne, F.C., Oberti, R., Ottolini, L. and Foord, E.E. (1996) Lithium-bearing fluor-arfvedsonite from Hurricane Mountain, New Hampshire: a crystal-chemical study. *The Canadian Mineralogist*, **34**, 1015–1019.

Hawthorne, F.C., Oberti, R., Cannillo, E., Ottolini, L., Roelofsen, J.N. and Martin, R.F. (2001) Li-bearing

https://doi.org/10.1180/minmag.2016.080.018 Published online by Cambridge University Press

arfvedsonitic amphiboles from the Strange Lake peralkaline granite, Quebec. *The Canadian Mineralogist*, **39**, 1161–1170.

Holness, M.B. and Sawyer, E.W. (2008) On the pseudomorphing of melt-filled pores during crystallization of migmatites. *Journal of Petrology*, **49**, 1343–1363.

Holness, M.B., Anderson, A.T., Martin, V.M., Maclennan, J., Passmore, E. and Schwindinger, K. (2007) Textures in partially solidified crystalline nodules: a window into the pore structure of slowly cooled mafic intrusions. *Journal of Petrology*, **48**, 1243–1264.

Jeffery, A.J. (2016) *Petrogenesis and contrasting eruption styles of peralkaline silicic magmas from Terceira and São Miguel, Azores*. Unpublished PhD thesis, Keele University, UK.

Khomyakov, A.P. (1995) *Mineralogy of Hyperagpaitic Alkaline Rocks.* Oxford Science Publications, Oxford, UK, 222 pp.

Konev, A.A., Vorob'ev, E.I. and Lasebnik, K.A. (1996) *The Mineralogy of the Murun Alkaline Massif.* Siberian Branch of the Russian Academy, Scientific Press, Novosibirsk [in Russian].

Krause, D.C. and Watkins, N.D. (1970) North Atlantic crustal genesis in the vicinity of the Azores. *Geophysical Journal of the Royal Astronomical Society*, **19**, 261–283.

Kröger, F.A. and Vink, H.J. (1956) Relations between the concentrations of imperfections in crystalline solids. *Solid State Physics*, **3**, 307–435.

Lazebnik, K.A. and Makhotko, V.F. (1982) Dalyite, the first finding in the USSR. *Zapiski Vsesoyuznogo Mineralogicheskogo Obschestva*, **111**, 587–593.

Lee, M.R. and Parsons, I. (1997) Dislocation formation and albitization in alkali feldspars from the Shap granite. *American Mineralogist*, **82**, 557–570.

Linthout, K., Nobel, F.A. and Lustenhouwer, W.J. (1988) First occurrence of dalyite in extrusive rock. *Mineralogical Magazine*, **52**, 705–708.

Mariano, A.N. and Francis, C.A. (1989) Dalyite from fenites in carbonatite complexes of the Minas Gerais – Goias belt, Brazil. *Geological Society of America Abstract Programs*, **21**, A46.

Mariano, A.N. and Marchetto, M. (1991) Serra Negra and Salitre – carbonatite alkaline igneous complex. Pp. 75–79 in: *5th International Kimberlite Conference (Field Guide Book)* (O.H. Leonardos, H.O.A. Meyer and J.C. Gaspar, editors). Araxá, Brazil, CPRM, Special publication, 3/91.

Marks, M.A.W., Hettmann, K., Schilling, J., Frost, B.R. and Markl, G. (2011) The mineralogical diversity of alkaline igneous rocks: critical factors for the transition from miaskitic to agpaitic phase assemblages. *Journal of Petrology*, **52**, 439–455.

Melia, T.P. and Moffitt, W.P. (1964) Crystallisation from aqueous solution. *Journal of Colloid Science*, **19**, 433–447.

Mitchell, R.H. and Bergman, S.C. (1991) *Petrology of Lamproites*. Plenum Press, New York/London, 447 pp.

Mujaji, M., Burrows J. and Jackson, R.A. (2014) Optical spectroscopy of the Nd^{3+} and Nd^{3+} – Gd^{3+}/Yb^{3+} centres in BaF_2 single crystals and calculations on lanthanide-doped BaF_2. *Journal of Luminescence*, **151**, 106–110.

Putnis, A. and Mauthe, G. (2001) The effect of pore size on cementation in porous rocks. *Geofluids*, **1**, 37–41.

Putnis, A., Prieto, M. and Fernandez-Diaz, L. (1995) Supersaturation and crystallisation in porous media. *Geological Magazine*, **132**, 1–13.

Raade, G. and Mladeck, M.H. (1983) Janhaugite, $Na_3Mn_3Ti_2Si_4O_{15}(OH,F,O)_3$, a new mineral from Norway. *American Mineralogist*, **68**, 1216–1219.

Reguir, E. (2001) *Aspects of the mineralogy of the Murun alkaline complex, Yakutia, Russia.* MSc thesis, Lakehead University, Canada, 193 pp.

Ridolfi, F., Renzulli, A., Santi, P. and Upton, B.G.J. (2003) Evolutionary stages of crystallization of weakly peralkaline syenites: evidence from ejecta in the plinian deposits of Agua de Pau volcano (Sao Miguel, Azores Islands). *Mineralogical Magazine*, **67**, 749–767.

Robins, B., Furnes, H. and Ryan, P. (1983) A new occurrence of dalyite. *Mineralogical Magazine*, **47**, 93–94.

Saleh, G.M. (2006) Geologic relationships and mineralisation of peralkaline/alkaline granite-syenite of the Zargat Na'am ring complex, Southeastern Desert, Egypt. *Chinese Journal of Geochemistry*, **25**, 97–111.

Salvi, S. and Williams-Jones, A.E. (1995) Zirconosilicate phase relations in the Strange Lake (Lac Brisson) pluton, Quebec-Labrador, Canada. *American Mineralogist*, **80**, 1031–1040.

Salvioli-Mariani, E. and Venturelli, G. (1996) Temperature of crystallisation and evolution of the Jumilla and Cancarix lamproites (SE Spain) as suggested by melt and solid inclusions in minerals. *European Journal of Mineralogy*, **8**, 1027–1039.

Scherer, G.W. (1999) Crystallization in pores. *Cement and Concrete Research*, **29**, 1347–1358.

Schmitt, A.K., Emmermann, R., Trumbull, R.B., Bühn, B. and Henjes-Kunst, F. (2000) Petrogenesis and $^{40}Ar/^{39}Ar$ geochronology of the Brandberg Complex, Namibia: evidence for a major mantle contribution in metaluminous and peralkaline granites. *Journal of Petrology*, **41**, 1207–1239.

Self, S. (1974) *Recent volcanism on Terceira, Azores.* PhD thesis, Imperial College, UK, 236 pp.

Self, S. (1976) The recent volcanology of Terceira, Azores. *Journal of the Geological Society*, **132**, 645–666.

https://doi.org/10.1180/minmag.2016.080.018 Published online by Cambridge University Press

Stepnova, Y.A., Zalishchak, B.L. and Pakhomova, V.A. (2013) Rare-earth mineralisation of alkali magma of the Russian Far East: on the example of the Shibanovsky massif. *Геология, Вестник,* **3**, 44–51 [in Russian].

Van Tassel, R. (1952) Dalyite, a new potassium zirconium silicate, from Ascension Island, Atlantic. *Mineralogical Magazine*, **29**, 850–857.

Venturelli, G., Capedri, S., Di Battistini, G., Crawford, A., Kogarko, L.N. and Celestini, S. (1984) The ultra-potassic rocks from southeastern Spain. *Lithos*, **17**, 37–54.

Widom, E., Gill, J.B. and Schmincke, H.-U. (1993) Syenite nodules as a long-term record of magmatic activity in Agua de Pau volcano, São Miguel, Azores. *Journal of Petrology*, **34**, 929–953.

https://doi.org/10.1180/minmag.2016.080.018 Published online by Cambridge University Press